Synthesis and characterization of membranes hemodialysis

Jennifer Gildo Alberto[1,2,3], María Teresa Viciosa[3], Maria Norberta Pinho[1,2]

[1] Centro de Fisica e Engenharia de Materiais Avançados (CeFEMA), Instituto Superior Técnico, Universidade de Lisboa.
[2] Departamento de Engenharia Quimica, Instituto Superior Técnico, Universidade de Lisboa.
[3] Centro de Química Estrutural - Institute of Molecular Sciences, Instituto Superior Técnico, Universidade de Lisboa.

*** Corresponding author email address**: jennifer.alberto@ulisboa.pt

Abstract

Mixed matrix membranes of cellulose acetate (CA) and silica (CA/SiO_2) were synthetized by coupling the wet phase inversion technique and the sol-gel method. Other set of CA based membranes were synthesized by direct mixing of the metal organic framework (MOF) UiO66 in the casting solution of the CA and CA/SiO_2 membranes (CA_UiO66 and CA/SiO_2_UiO66 respectively).
The physical and chemical properties of the membranes were investigated by Differential Scanning Calorimetry (DSC) and Dielectric Relaxation Spectroscopy (DRS). The former allowed determining parameters such as the crystallinity degree and the glass transition temperature (T_g). On the other hand, DRS was used to analyze the molecular dynamics of each CA based membranes in the sub-T_g temperature region; the different relaxation processes detected were interpreted considering the interactions of membranes with water.
Permeation experiments were carried out in an ultrafiltration set-up for the CA, CA/SiO_2, CA_UiO66 and CA/SiO_2_UiO66. Their permeation characteristics in terms of hydraulic permeabilities, molecular weight cut-off (MWCO), and apparent rejection coefficients to NaCl, Na_2SO_4, urea, and p-cresyl sulphate and p-cresyl with albumin (BSA) were determined.
The membranes selective performance was correlated with the characterization parameters**.**

Keywords: Monophasic hybrid membranes, Cellulose acetate/silica, Metal organic framework, Ultrafiltration, Dielectric relaxations, Permeability.

1. Introduction

Chronic kidney disease (CKD) has been one of the biggest concerns in the medical world in recent years and is expected to rise over the next decades [1]. This disease affects 11-13% of the population worldwide [2].
This disease is related to the accumulation of uremic toxics that can lead to end stage renal disease (ESRD). Patients that reach the ESRD-stage, may be subjected to a renal replacement therapy (hemodialysis) or transplantation. Transplantation depends on finding compatible healthy kidney donors and the procedure may put the patient under various risks. Hemodialysis (HD) has been the most viable route for this type of disease. Hemodialysis is the renal replacement therapy where blood purification is employed to take out metabolic leftovers that accumulate in the blood of patients with ESRD. Semi-permeable membranes are arranged in a compact fashion known as membrane module it provides the setup of channels for the counter-current flows of blood and dialysate fluids. A membrane is the core component of the HD machine, for the extracorporeal treatment [1,3].
Toxin elimination from blood can reduce problems and increase survival time in dialysis patients. However, Protein-Bound Uremic Toxins (PBUTs) are difficult to eliminate during conventional H) since they bind preferentially to proteins. Protein-Bound Uremic Toxins clearances would be improved if there are binding sites competitive to the ones of the plasma proteins. The uremic toxins, including, indoxyl sulfate p-cresyl sulfate, and hippuric acid (PTUBs) primarily bind to the human serum albumin (HSA) in human blood and they have an aromatic moiety and an ionic functional group, allowing electrostatic and/or van der Waals forces to attach to numerous adsorption sites on HAS [4]. So, these interactions prevent the efficient removal of PBUTs through conventional extracorporeal renal replacement therapies, such as a hemodialysis.

In general, protein-bound uremic toxins (PBUTs) have molecular weights (MW) smaller than 500 Da but are difficult to remove through most dialytic procedures because of their high plasma protein binding, especially to human serum albumin (HSA; MW 65.5 kDa). PBUTs circulate in the bloodstream in the form of bound and unbound, or free, fractions. The concentration of bound toxins is variable and depends on the binding affinity to plasma proteins, such as HAS.

2. Materials

Membranes were synthesized with cellulose acetate (CA, $C_6H_7O_2(OH)_3$, ~30 000 $gmol^{-1}$) with degree of acetylation of 39.8% from Sigma-Aldrich, formamide (CH_3NO, 45.02 $gmol^{-1}$, Panreac), pure acetone (C_3H_6O, 58.08 $gmol^{-1}$, purity ≥ 99.7%, José M. dos Santos, LDA), tetraethyl orthosilicate (TEOS), $Si(OC_2H_5)_4$ (208.33 $gmol^{-1}$, reagent grade 98%, Alfa Aesar), nitric acid (HNO_3, 63.01 $gmol^{-1}$, 65% v/v, Chem-Lab) and metal organic framework (MOF) UiO66 ($Zr_6O_4(OH)_4(C_6H_4C_2O_4)_6$, 1664.1 $gmol^{-1}$, synthesized in laboratory [5].
Molecular weight cut-off (MWCO) was studied using polyethylene glycol (PEG) 3000 (2000 $gmol^{-1}$, Merck),

PEG 6000 (6000 $gmol^{-1}$, Merck), PEG 10000 (10000 $gmol^{-1}$, Merck), PEG 20000 (20000 $gmol^{-1}$, Merck), PEG 35000 (35000 $gmol^{-1}$, Merck), PEG 40000 (40000 $gmol^{-1}$, Merck). Permeation experiments were carried out with sodium chloride (NaCl, 58.44 $gmol^{-1}$, Panreac), urea ($CO(NH_2)_2$), 60.06 $gmol^{-1}$, Merck), potassium p-cresyl sulphate (PCs, $C_7H_7KO_4S$, 226.29 $gmol^{-1}$, synthesized by Prof. J. P. Telo following ref. [6]), bovine serum albumin (BSA, ~66500 $gmol^{-1}$, SigmaAldrich).

2.1 Membrane synthesis

CA, CA/SiO_2, CA_UiO66, and CA/SiO_2_UiO66 membranes were synthesized by combining the processes of wet phase inversion, sol-gel, and direct MOF dispersing while maintaining a constant composition of SiO_2 and UiO66. The direct MOF blending approach was used to incorporate UiO66 in the membranes [7]. A polymer solution, or casting solution, containing cellulose acetate (CA, polymer), acetone (stronger/good solvent), and formamide (weaker solvent), is required for the phase inversion process.

Following the sol-gel process, the SiO_2 alkoxide sol-gel precursor, TEOS, was added and hydrolyzed by adding water and nitric acid to the casting [8]. The MOF UiO66 was directly added to the CA and CA/SiO_2 casting solutions.

Table 1. Casting solutions composition in w/w % for membrane syntheses. * TEOS is the precursor SiO_2 agent.

	CA	**CA/SiO_2**	**CA_UiO66**	**CA/SiO_2_ _UiO66**
CA	17	16.4	16.8	16.2
Formamide	22	21.3	21.8	21
Acetone	61	58.84	60.4	58.3
H_2O	-	0.5	-	0.5
TEOS *	-	3	-	3
UiO66	-	1	1	1
HNO_3	-	4 drops (pH~2)	-	4 drops (pH~2)

2.3 Differential scanning calorimetry (DSC)

The thermal features were examined using differential scanning calorimeter DSC Q2000 from TA Instruments Inc. (Tzero DSC technology) operating in the Heat Flow T4P option. Enthalpy (cell constant) and temperature calibration were based on the melting peak of indium standard (T_m = 156.60 °C). Membranes were cut into small pieces (approximately 5 mg) and introduced in an aluminium hermetic pan with a Tzero hermetic lid with a pinhole to facilitate the exit of water. Thermograms of all the membranes were obtained over a range of -80 °C to 240 °C at a heating rate of 5 °Cmin^{-1} under a nitrogen flow of 50 mLmin^{-1}. Cooling ramps were conducted in the conventional mode while heating runs were done in the modulated one (modulated parameters: amplitude, A = ±0.663 °C, period, p = 50 s).

The data analyses were carried out using the software Universal Analysis 2000 from TA Instruments.

2.4 Dielectric Relaxation Spectroscopy (DRS)

ALPHA-N impedance analyzer from Novocontrol Technologies GmbH, covering a frequency range from 0.1 Hz to 1 MHz. Each membrane sample was cut into a disk with thickness ~ 0.045 mm which was placed between two gold-plated electrodes of a parallel plate capacitor, BDS 1200. The sample cell was mounted on a BDS 1100 cryostat and exposed to a heated gas stream being evaporated from a liquid nitrogen dewar. The temperature was controlled by Quatro Cryosystem and performed within 0.5 K. The measurements start with a cooling ramp at 5 °Cmin^{-1}, from 20 °C to -120 °C, with data continuously taken at five selected frequencies (10^2, 10^3, 10^4, 10^5 and 10^6 Hz). After that, in steps of 5 °C, isothermal measurements covering the frequency range from 0.1 to 10^6 Hz were carried from -120 °C to 100 °C (series 1) and then from -120 °C to 200 °C (series 2).

$$\varepsilon^*(\omega) = \varepsilon'(\omega) - i\varepsilon''(\omega) \qquad \text{Equation 1}$$

Due to the high conductivity contribution observed, spectra will be analysed by the dielectric modulus representation, being this related to complex permittivity as $M^* = 1/\varepsilon^*$.

Data analysis

To analyze the isothermal dielectric data, the Havriliak-Negami (HN) model function [9,10] was fitted to both imaginary and real components of the electrical modulus, M*(ω). To account for the multimodal profile, a sum of HN functions was considered:

$$M^*_{HN}(\omega) = M_\infty + \sum_j \frac{\Delta M}{(1 + (-i(\omega\tau_{HN})^{-1})^{\alpha_{HN}})^{\beta_{HN}}} \qquad \text{Equation 2}$$

where j is the index over which the individual processes are summed, $\Delta M = M_0 - M_\infty$, τ_{HN} is the characteristic HN relaxation time, and α_{HN} and β_{HN} are shape parameters ($0 < \alpha_{HN} < 1$ and $0 < \alpha_{HN}\,\beta_{HN} \leq 1$) describing, respectively, the symmetric and asymmetric broadening of the complex dielectric function [11].

From the estimated values of τ_{HN} and the shape parameters, a model-independent relaxation time was determined from [11]:

$$\tau_{max} = \tau_{HN}\left[sin\left(\frac{\alpha_{HN}\pi}{2+2\beta_{HN}}\right)\right]^{-\frac{1}{\alpha_{HN}}}\left[sin\left(\frac{\alpha_{HN}\beta_{HN}\pi}{2+2\beta_{HN}}\right)\right]^{-\frac{1}{\alpha_{HN}}}$$ Equation 3

The temperature dependence of relaxation times could be described by the Arrhenius equation in the case of thermal activated processes (linear T-dependence) that reads:

$$\tau = \tau_0 exp\left(\frac{E_a}{RT}\right)$$ Equation 4

where τ_0 is the relaxation time at infinite T, R is the ideal gas constant and E_a is the activation energy.

3. Results and Discussion

This section starts with the physical characterization of the membranes by DSC and DRS, and then it continues presenting the results regarding the permeability parameters. A discussion will be provided as the different results are included.

3.1 Differential scanning calorimetry results

The calorimetric analysis will be presented firstly for CA membrane, and then a comparison for all the membranes will be presented.

CA membrane without any additional treatment was initially cooling from 20 °C to -80 °C; the corresponding thermogram is displayed in Figure 1a (black line). A large exothermal event is visible whose onset is close to -18 ºC that can be associated to the crystallization of bulk water in the sample. At lower temperatures, close -40 °C, another small peak is observed (see vertical arrow in Figure 1a) that may be related to a water fraction deeper located in the membrane. On the subsequent heating, the melting of crystalline water begins close to -18 ºC (black line in Figure 1b) and presents a minimum at -1.03 ºC.

Above room temperature, a large exothermal peak is observed with minimum at 100.2 ºC, corresponding to the water release. Close to 200 ºC, the heat flow shows a step indicating the glass transition (of the dried membrane) (inset in Figure 1) whose onset was found at 194.4 ºC. Immediately above the glass transition, an additional exothermal peak is detected (T_{min} = 224.9 °C) that can be associated to the melting of the crystalline fraction of the CA membrane. The enthalpy calculated from the thermogram was ΔH_m = 8.4 Jg^{-1} (this value was corrected considering the water loss during the measurement). From this value is possible to estimate the crystallinity degree by the ratio between the melting enthalpy of the material under study (ΔH_m) and the respective value for the totally crystalline material, ($\Delta H°_m$ = 58.8 Jg^{-1} [12]), by the next equation:

$$X_c(\%) = \frac{\Delta H_m}{\Delta H_m^\circ} \times 100$$ Equation 5

For CA membrane the crystallinity degree estimated by this way was χ_c = 14.2 %, very similar to that found in a similar asymmetric CA membrane [13].

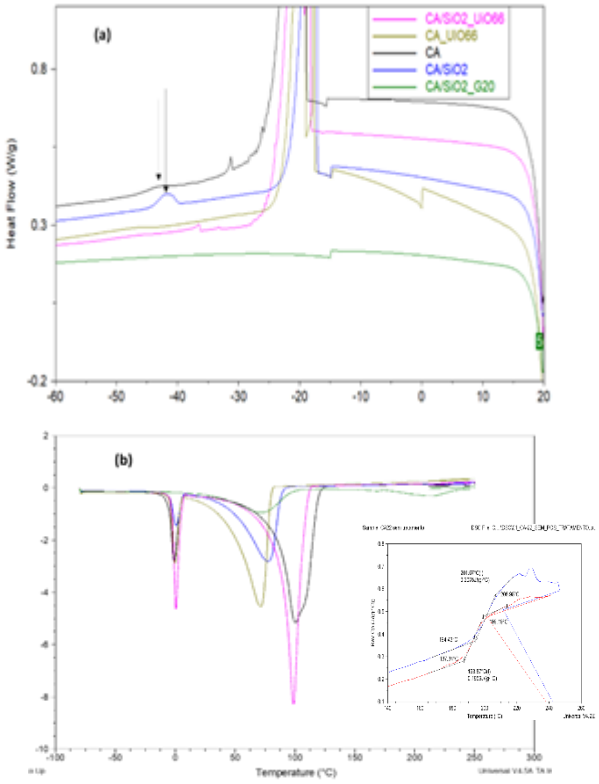

Figure 1. Heat flow thermograms obtained at 5 ºCmin^{-1} (a) on cooling, and (b) on heating under modulated conditions (amplitude = ±0.663 ºC and period = 50 s), for CA, CA/SiO_2, CA_UiO66 and CA/SiO_2_UiO66 membranes. Inset: Reversible component of the heat capacity obtained during first and second heating of CA membrane in the glass transition region.

During posterior cooling and subsequent heating, only the glass transition signal was observed. The $T_{g\text{-}onset}$ in the second heating was shifted to lower temperatures, 187. 3 ºC (red line in the inset in **Erro! A origem da referência não foi encontrada.**b) that suggesting that the presence of a crystalline fraction leads to a constrained amorphous polymer.

The variation of the heat capacity (ΔC_p) as result of the increase of the degree of freedom at glass transition is 1.82 $J(Cg)^{-1}$ (corrected with the water loss).

Hybrid membranes with SiO_2 and/or UiO66 present similar thermal events. It can be highlighted the more pronounced exothermal peak in CA/SiO_2 membrane close to -42 ºC (see vertical arrow in Figure 1a pointing to blue line). On the other hand, while water melting on heating occurs at similar temperatures for all the membranes, some

differences are detected in the T_{min} related to water evaporation (see values on Table 2); from the comparison with CA, the hybrid membrane (CA/SiO_2) and that with MOF incorporated show a lower T_{min}, indicating weaker water-membrane interactions.

Table 2. Glass transition temperature (T_g) determined in the onset, heat capacity change at T_g (ΔC_p) (with mass correction), and the corrected values according to the mass loss for CA, CA/SiO_2, CA_UiO66 and CA/SiO_2_UiO66 membranes.

	CA	**CA/SiO_2**	**CA_UiO66**	**CA/SiO_2_ UiO66**
T_{min} (ºC) evaporation	100.4	77.9	71.4	98.8
χ_c (Jg^{-1})	14.2	27.8	7.8	10.2
$T_{g\text{-}on}$ (°C)	187.6	188.8	183.5	188.7
ΔC_p ($J(g°C)^{-1}$)	1.82	1.21	0.70	0.24

Regarding the crystallinity degree is significant the increase observed in the CA_SiO_2 membrane which suggests that the presence of SiO_2 promotes the crystallization of CA.
The glass transition temperature (taken on the second heating run) presents similar values (see Appendix 1) meaning that either the presence of covalent bounded SiO_2 and/or dispersed UiO66 has not significant influence on this parameter.

3.2 Dielectric relaxation spectroscopy results

As in calorimetric measurements, membranes were submitted to a cooling ramp from 20 ºC to -80 ºC at 5 $ºCmin^{-1}$. The permittivity values obtained in this cooling ramp are represented in Figure 2a for four selected frequencies for CA membrane. From the comparison with the corresponding heat flow thermogram (Figure 2b) it can be identified two changes in the slope very close to the exothermal events associated to the crystallization of water. These results will be further discussing in the text.
On the subsequent heating, isothermal spectra were collected every five degrees up to 100 ºC; then, the sample was cold down to -120 ºC and a second series of isothermal spectra were monitored up to 200 ºC. In Figure 3 it is represented the isochronal dielectric modulus (M´´) values at the frequency of 10^3 Hz for the two series (note that every isothermal spectrum spends approximately 10 minutes, resulting in an equivalent heating rate around 0.5 $ºCmin^{-1}$).
From DSC analysis, it was shown that bulk water recrystallizes on cooling ramp. This phenomenon is also observed in dielectric results by a decrease in M´´ (and ε´´) close to -30 °C.

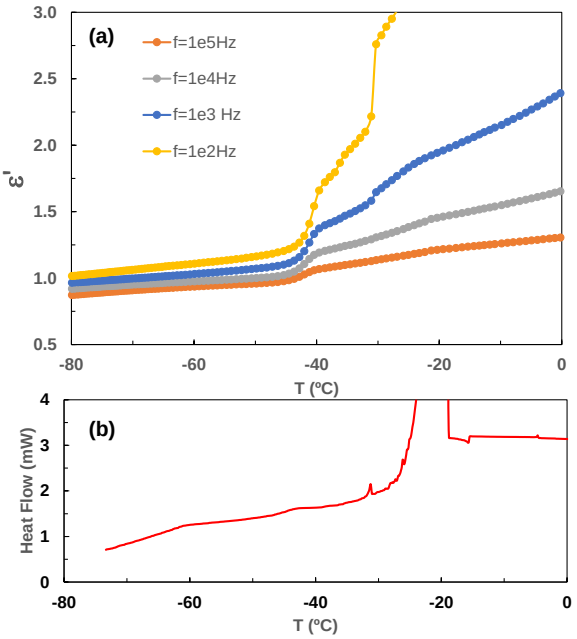

Figure 2. (a) Real part of complex permittivity for four frequencies indicated in the figure, and (b) heat flow thermogram obtained on cooling at 5 $ºCmin^{-1}$.

With continuous cooling, the ε´´(T) trace allows distinguish at least one dipolar relaxation close below -100 °C. On the first heating (yellow circles in Figure 3), the obtained values of M´´(f) are identical up to -45 ºC, and significant differences are observed above this temperature; this is not surprising if we take into account the previous results observed by DSC from which crystallization (on cooling) and melting (on heating) don't occur at the same temperatures.
At higher temperatures, close to 50 °C, during first series, a sharp decrease is observed in M´´(f) which corresponds to the water evaporation (i.e. a large decrease in the dipolar/conductivity answer of the sample). During the second series, only a very large relaxation is observed (blue data in Figure 3).

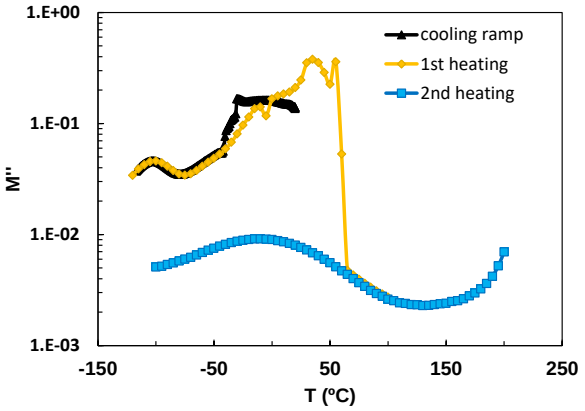

Figure 3. Imaginary part of complex dielectric modulus (M´´) for CA membrane at 10^3 Hz.

To obtain reliable information about the dynamical behaviour of the CA membrane, it is useful to pay attention to isothermal spectra acquired on heating. Examples of M´´(f) spectra for series 1 are presented in Figure 4 in which multiple peaks can be directly seen.

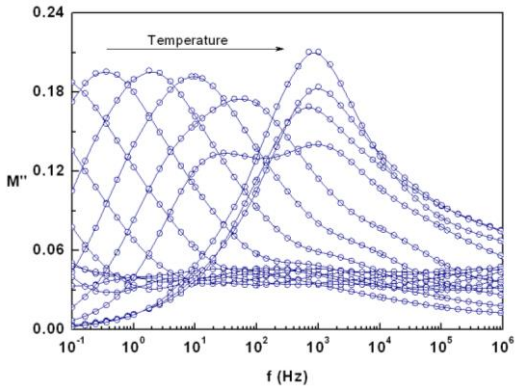

Figure 4. Imaginary part of complex dielectric modulus (M´´) for CA membrane for temperatures from -55 to 5 ºC every 5 ºC.

In order to determine the characteristic relaxation times of each process, isothermal spectra were deconvoluted in the individual relaxations by using a sum of HN equations (imaginary component). Examples of this data treatment are included in following figure for spectra collected at -100, -50 and 0 °C.

By this data treatment up to six relaxations were distinguished whose shift to higher frequencies as the temperature increases. In Appendix 2 are summarized the α_{HN} and β_{HN} fitting parameters used for all the relaxations detected. Regarding the characteristic relaxation time, τ_{HN}, the main parameter obtained from the fitting, it was converted to the model-independent, τ_{max} by Equation 3.
The relaxation times estimated by this way have been represented against the reciprocal temperature in Figure 6 from which the most relevant features are:

(i) all processes follow a linear temperature dependence that can be well described by an Arrhenius-type equation, whose activation energies and pre-exponential factor are included in Table 3;
(ii) as temperature increases, process 1 tend to merge with process 2 (see yellow arrow in Figure 6) suggesting a similar origin;
(iii) process 3 and 4 undergoes a change from a linear trend to another with a high slope at around T~ -3 °C (~3.7 = 1000/T(K)), probably related to water melting.

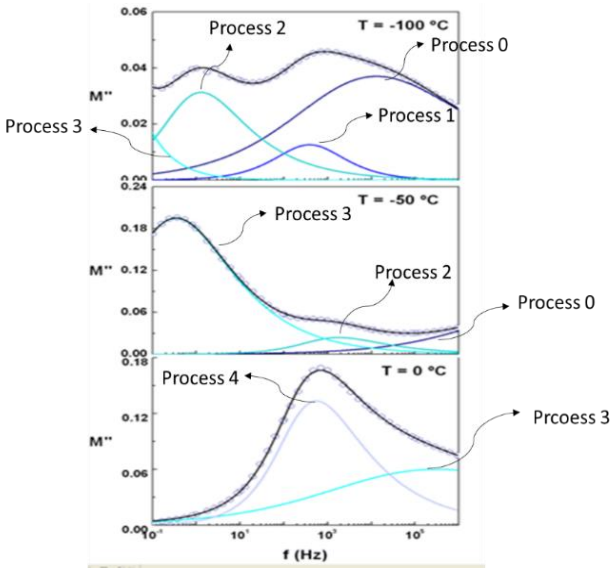

Figure 5. Isothermal M´´ spectra at -100, -50 and 0 ºC (open symbols) and the individual HN fitting functions (blue lines) to describe the raw data (black line is the overall fitting function).

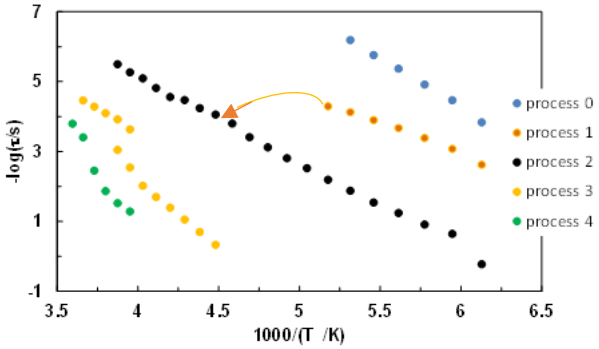

Figure 6. Relaxation map obtained for CA membrane.

Table 3. Activation energy E_a (kJmol^{-1}) and pre-exponential factor (τ_0) values obtained by fitting with Equation 4.

	Process 0	Process 1	Process 2	Process 3	Process 4
E_a (kJmol^{-1})	54.2	33.1	46.9	86.3	51.1
τ_0 (s)	5.6×10^{-22}	4.9×10^{-14}	1.1×10^{-15}	4.4×10^{-21}	5.9×10^{-15}

In the second series of isothermal spectra, only one broad peak was observed as it can be seen in Figure 7. The reduction of relaxations modes from 5/6 to one leads to assume that the processes observed in the initial state are mainly due to the presence of water, while that remaining in the second series can be undoubtedly ascribed to localized motions in the CA matrix (note heated above 200 ºC, the sample must be totally dehydrated and probably the initial porosity must be destroyed).

Regarding the hybrid membranes and those with UiO66 incorporated, the M´´ (or ε´´) isochronal representation shows significant differences when compared with CA. At lowest temperatures two maxima are clearly distinguished at -105 ºC and -60 ºC, approximately. On the other hand, a sharp decrease is observed close to 0 ºC in these membranes and the change ascribe to water evaporation is detected at higher temperatures than in CA.

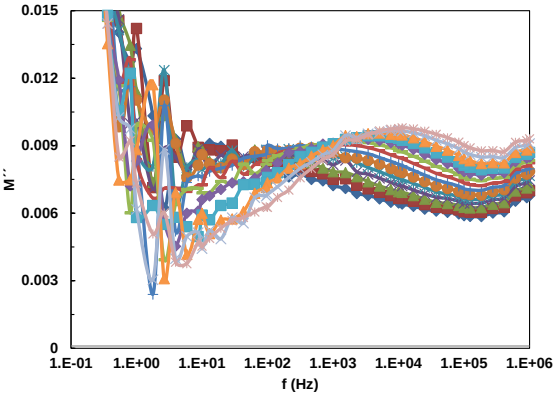

Figure 7. Isothermal spectra collected from -55 to 10 ºC (every 5 degrees) in the second series, i.e. once the sample has been heated at 100 ºC, for CA membrane.

In the second series CA/SiO_2 and CA_UiO66 shows a similar profile that CA, i.e. a broad and low intense relaxation, while CA/SiO_2_UiO66 exhibits two maxima. The analysis of the second isothermal data spectra is not included in this manuscript.

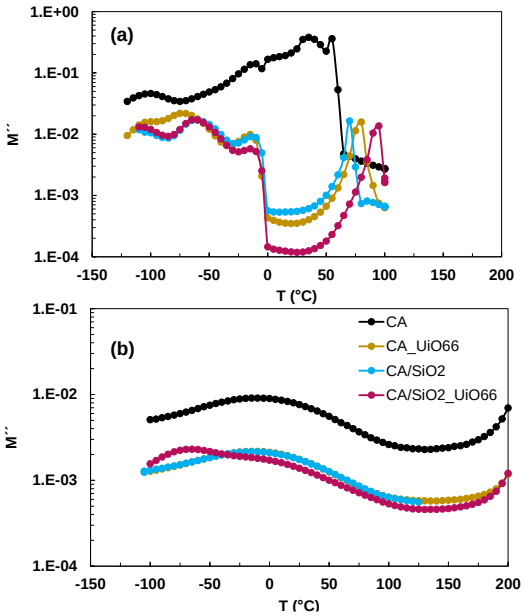

Figure 8. Isochronal representation of dielectric modulus (M´´) at f = 10^3 Hz of CA (black), CA_UiO66 (yellow), CA/SiO_2 (blue) and CA/SiO_2_UiO66 (red) membranes: (a) first heating and (b) second heating.

Isothermal M´´(f) spectra in these samples were analysed following the same procedure to that applied for CA (the corresponding fitting parameters are included in Appendix 2).

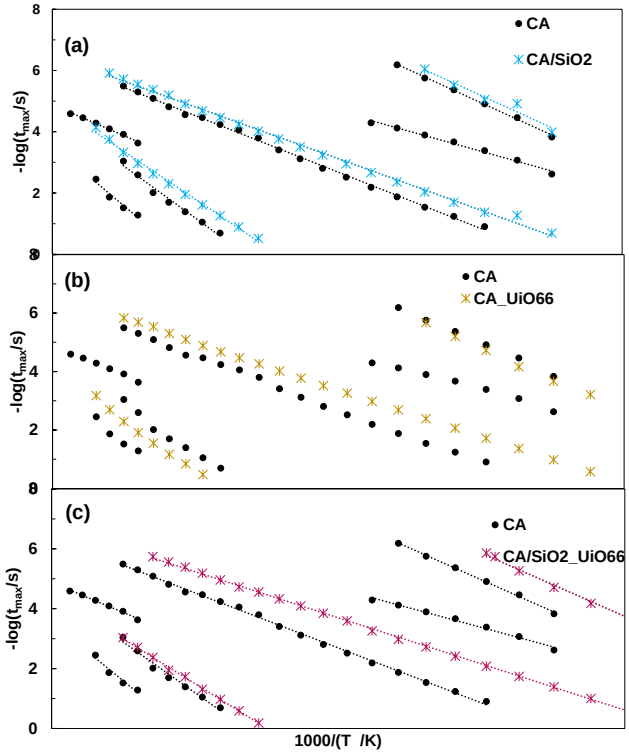

Figure 9. Relaxation map of: (a) CA/SiO_2, (b) CA_UiO66 and (c) CA/SiO_2_UiO66 membranes. CA results are included as black symbols for comparison.

As it was found in CA membrane, all the detected relaxations follow a linear temperature dependence in the relaxation map (Figure 9) that can be described by Equation 4. The corresponding activation energies and pre-exponential values are included in Table 4.

Table 4. Activation energy E_a (kJmol^{-1}) and pre-exponential factor (τ_0) values obtained by fitting with Equation 4 for three common relaxations detected in CA, CA/SiO_2, CA/UiO66 and CA/SiO_2_UiO66 membranes.

	Process I		Process II		Process III	
	E_a (kJmol^{-1})	τ_0 (s)	E_a (kJmol^{-1})	τ_0 (s)	E_a (kJmol^{-1})	τ_0 (s)
CA	54	5.0×10^{-22}	47	1.1×10^{-15}	86	4.4×10^{-21}
CA/SiO_2	54	3.6×10^{-22}	43	4.6×10^{-15}	77	1.1×10^{-19}
CA_UiO66	53	1.8×10^{-21}	39	1.3×10^{-14}	84	5.2×10^{-20}
CA/SiO_2_UiO66	54	9.2×10^{-22}	39	1.0×10^{-14}	75	2.6×10^{-19}

It can be concluded from these parameters that: (i) process I is nearly unaffected by the presence of SiO_2 or UiO66; (ii) the activation energies of process II and III decreases for hybrid membrane and for that with MOF incorporated. These changes may be related to the way as water is distributed in the sample or in other words, in how it is

interacting with the membrane (and SiO_2 and MOF groups).

3.3 Hydraulic permeability

The hydraulic permeability (L_p) was determined for each membrane by representing graphically the pure water permeation fluxes, J_w (corrected at 25 ºC), as function of transmembrane pressures which varying from 0.5 to 4 bar. The slope of each linearization's represented in Figure 10 corresponds to hydraulic permeability estimated for each membrane; the obtained values have been summarized in Table 5.

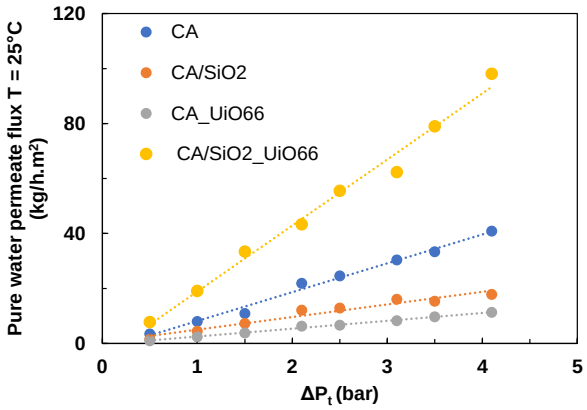

Figure 10. Pure water permeate mass flux at 25 °C as a function of the applied transmembrane for each membrane. The permeate fluxes were measured at a volumetric feed flow rate of 2.5 $Lmin^{-1}$ and with a membrane surface area of 13.2×10^{-4} m^2.

As it can be seen hybrid membrane and that with MOF incorporated decreases the permeability values, while in the more complex membrane, CA/SiO_2_UiO66, the opposite is observed.

Table 5. Hydraulic permeability and molecular weight cut-off of CA, CA/SiO_2, CA_UiO66 and CA/SiO_2_UiO66 membranes.

	L_p ($Kg(hm^2bar)^{-1}$)	**MWCO (kDa)**
CA	10	22
CA/SiO_2	5	14
CA_UiO66	3	8
CA/SiO_2_UiO66	22	19.5

Molecular weight cut off (MWCO)

For MWCO determination, the ultrafiltration is carried out for aqueous solutions of PEG with increasing molecular weight: 3kDa, 6 kDa, 10 kDa, 20 kDa, 35 kDa and 40 kDa.

To determine the MWCO, the apparent rejection coefficient to PEG solutes is plotted as a function of the PEG molecular weight; then, the intersection of the curve describing this behavior with the apparent rejection coefficient at 91% provides an estimated value for the molecular weight cut-off (Figure 11).

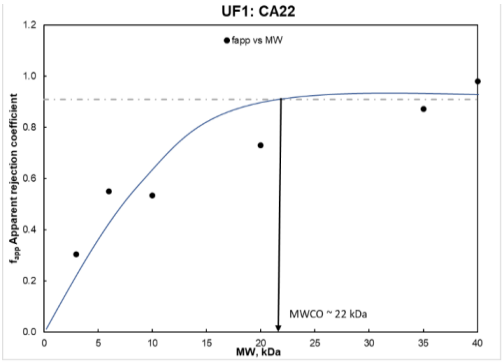

Figure 11. CA membrane apparent rejection coefficient vs. solute PEG molecular weight. Aqueous solutions with a feed concentration of 0.6 gL^{-1} for PEG's: 3, 6, 10, 20, 35 and 40 kDa, at ΔP_t = 1bar at the maximum volumetric feed flow rate, 3 $Lmin^{-1}$, and a membrane surface of 13.2×10^{-4} m^2.

From the comparison with the MWCO of CA membrane(Table **5**), it is clear that for hybrid CA/SiO_2 membrane reduces from 22 to 8 kDa. Regarding the effect of introducing MOF in CA or in CA/SiO_2, the are not a clear effect associated since it decreases when added to CA (from 22 to 8 kDa) and increases when it is incorporated in CA/SiO_2 (from 14 to 19.5 kDa).

Apparent rejection coefficient to salts

The apparent rejection coefficients, f_{app}(%), to NaCl and Na_2SO_4 were used to assess the selectivity of each membrane. All the permeation experiments were conducted at the maximum volumetric feed flow rate (3.27 $Lmin^{-1}$) which corresponds to the maximum volumetric velocity. The apparent rejection was determined with solutions of 0.6 g/L at 1 bar.

Table 6. Apparent rejection coefficients of salts (%).

	CA	CA/SiO_2	CA_UiO66	CA/SiO_2_UiO66
NaCl	12	45	39	4
Na_2SO_4	11	60	28	6

Results summarized in Table 6 shown that these salts are partially rejected by membranes and the introduction of MOF influence this parameter. In CA membrane the apparent rejection coefficient (f_{app}) to salts is lower than CA with MOF (CA_UiO66) and CA/SiO_2 membrane is higher than CA/SiO_2_UiO66 membrane.
The greatest difference in the rejection of a monovalent salt or divalent salt is observed in CA/SiO_2 membrane.

Apparent rejection coefficient to uremic toxins

The apparent rejection coefficients, f_{app}, were determined over a pressure range from 0.5 to 3 bar for following solutions: 0.4 gL^{-1} of urea, 4.6 gL^{-1} of urea, 0.1 gL^{-1} of PCs, 0.5 gL^{-1} of BSA and 0.5 gL^{-1} of PCs and 0.1 gL^{-1} of PCs. In the last two cases, the apparent rejection refers to PCs.

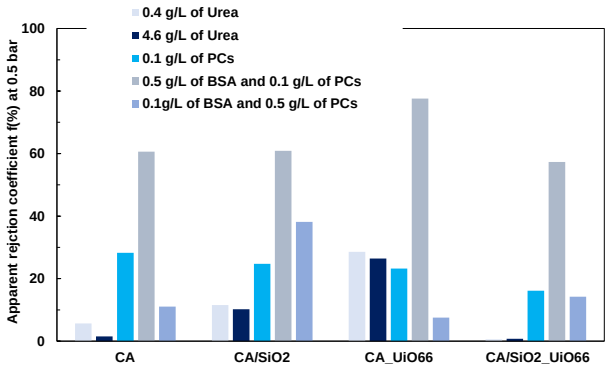

Figure 12. Apparent rejection coefficient (f) in percentage to urea, PCs and BSA-PCs at different concentrations for CA, CA/SiO_2, CA_UiO66 and CA/SiO_2_UiO66 membranes.

As it can see in Figure 12Figure **12**, the apparent rejections of CA, CA/SiO_2 and CA/SiO_2_UiO66 membranes to the urea solution (0.4 gL^{-1} and 4.6 gL^{-1}) are very low, i.e. there is practically no rejection. This result is expected given that urea is considered a small water-soluble compound [4]. On other hand, for CA_UiO66 membrane the rejection to urea is relatively high, principally in lowers transmembrane pressures.
The urea´s apparent rejection increases by adding UiO66 in CA membrane, as it is clearly seen immediately at the transmembrane pressure of 1 bar.

Relative to the last two scenarios where PCs is binding with BSA:

(i) in the case of 0.1gL^{-1} of PCs with 0.5gL^{-1} BSA, the apparent rejection of PCs are also higher comparing with the permeation of PCs solution only.

(ii) For 0.5 gL^{-1} of PCs with 0.1 gL^{-1} of BSA, the apparent rejection coefficients are lower. This decrease is expected because there is biggest free fraction of PCs.

4. Conclusions

CA and CA/SiO_2 membranes were successfully synthesized by combining phase inversion and sol-gel techniques. By direct incorporation of MOF UiO66 in the casting solutions, also CA_UiO66 and CA/SiO_2_UiO66 were obtained.

By Differential Scanning Calorimetry (DSC) it was shown that, on cooling, most of water recrystallizes at temperatures close to -18 ºC, as expected for bulk water. On the other side, water evaporation depends on the membrane, occurring at approximately 30 degrees below for CA/SiO_2 and CA_UiO66 membranes relative to CA. Relatively to the crystallinity degree it depends on the membrane composition following this order: CA/SiO_2 (28%), CA (14%), CA/SiO_2_UiO66 (10%) and CA_UiO66 (8%). Regarding the glass transition temperature, it is almost unaffected by the presence of SiO_2 and/or UiO66; on the other hand, it is shifted to lower values when CA are fully amorphous.

The molecular mobility was probed by dielectric relaxation spectroscopy (DRS). The main result refers to the reduction of the number of relaxation modes observed at lower temperatures, that changes from five detected in CA to three observed in hybrid membranes with or without UiO66. These relaxations are principally related to the water presence in the samples, given that after heating above 250 ºC, both number and intensity are significantly depleted in all studied membranes. All the detected relaxations follow an Arrhenius temperature dependence of the corresponding relaxation times.

Concerning membrane selective analysis, by introducing MOF in CA membrane the hydraulic permeability decreases, while in hybrid membrane CA/SiO_2, the opposite was observed.
Furthermore, by comparing the apparent rejection parameter for MW of small water-soluble compounds (urea and PCs) with the MWCO values higher than 6 kDa (polyethylene glycol, PEG), it is possible to anticipate that urea and PCs can be removed when they are not bounded to any protein.
Regarding the salts permeation, they are partially rejected by the membranes; the influence of introducing UiO66 MOF leads to reduces the apparent rejection coefficient (f_{app}) to salts, while increases when MOF it is incorporated in hybrid CA/SiO_2 membrane.

Acknowledgments

M. Dionísio for the facilities with the calorimetric and dielectric equipment.

Appendix

Appendix 1.

Thermograms obtained in the second heating at 5 ºCmin^{-1} (A = ±0.663 ºC, p = 50 s) for CA, CA/SiO_2, CA_UiO66 and CA/SiO_2_UiO66 membranes

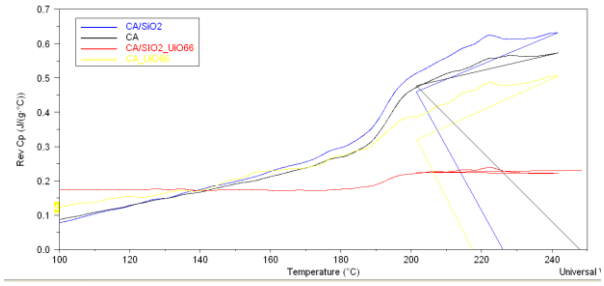

Appendix 2.

α_{HN} and β_{HN} fitting parameters for the common relaxation processes detected in the CA, CA/SiO_2, CA_UiO66 and CA/SiO_2_UiO66 membranes.

	CA		
	Process 0	Process 1	Process 2
α_{HN}	0.36	0.72	0.6
β_{HN}	0.6	0.55	0.5
T range (°C)	[-110,-60]	[-105,-15]	[-55,5]
	CA/SiO_2		
α_{HN}	0.36	0.7	0.8
β_{HN}	0.7	1	1
T range (°C)	[-110,-75]	[-110, 0]	[-55,5]
	CA_UiO66		
α_{HN}	0.69	0.4	0.63
β_{HN}	1	0.73	1
T range (°C)	[-120,5]	[-120,-85]	[-60,5]
	CA/SiO2_UiO66		
α_{HN}	0.63	0.7	0.4
β_{HN}	1	1	0.5
T range (°C)	[-60,5]	[-120,-5]	[-120,-90]

References

[1] T. Liyanage, T. Ninomiya, V. Jha, B. Neal, H. Patrice, I. Okpechi, M. H. Zhao, J. Lv, A. X. Garg, J. Knight, A. Rodgers, M. Gallagher, S. Kotwal, A. Cass, V. Perkovic. Worldwide access to treatment for end-stage kidney disease: a systematic review. *The Lancet* **2015**, 385(9981), 1975–1982. doi: 10.1016/S0140-6736(14)61601-9.

[2] N. R. Hill, S. T. Fatoba, J. L. Oke, J. A. Hirst, C. A. O'Callaghan, D. S. Lasserson, F. D. R. Hobbs, G. Remuzzi. Global Prevalence of Chronic Kidney Disease – A Systematic Review and Meta-Analysis. PLOS ONE **2016**, 11(7), 158–765. doi: 10.1371/journal.pone.0158765.

[3] S. U. Zaman, S. Rafiq, A. Ali, M. S. Mehdi, A. Arshad, S. U. Rehman, N. Muhammad, M. Irfan, M. S. Khurram, M. K. U. Zaman, A. S. Hanbazazah, H. R. Lim, P. L. Show. Recent advancement challenges with synthesis of biocompatible hemodialysis membranes. *Chemosphere* **2022**, 307(2), 135626. doi:10.1016/j.chemosphere.2022.135626.

[4] R. Vanholder, R. De Smet, G. Glorieux, A. Argilés, U. Baurmeister, P. Brunet, W. Clark, G. Cohen, P. P. De Deyn, R. Deppisch, B. Descamps-Latscha, T. Henle, A. Jörres, H. D. Lemke, Z. A. Massy, J. Passlick-Deetjen, M. Rodríguez, B. Stegmayr, P. Stenvinkel, C. Tetta, C. Wanner, W. Zidek. Review on uremic toxins: Classification, concentration and interindividual variability. *Kidney International* **2003**, 63(5), 1934–1943. doi: 10.1046/j.1523-1755.2003.00924.x.

[5] K. Dedecker, R. S. Pillai, F. Nouar, J. Pires, N. Steunou, E. Dumas, M. L. Pinto. (**2020**). Metal-Organic Frameworks for Cultural Heritage Preservation: The Case of Acetic Acid Removal. *ACS Appl. Mater. Interfaces* **2018**, 10, 16, 13886–13894. doi: 10.1021/acsami.8b02930

[6] J. Feigenbaum, C. A. Neuberg. Simplified Method for the Preparation of Aromatic Sulfuric Acid Esters. *Am. Chem. Soc.* **1941**, 63, 12, 3529–3530. doi: 10.1021/ja01857a508

[7] Y. Deng, Y. Wu, G. Chen, X. Zheng, M. Dai, C. Peng. Metal-organic framework membranes: Recent development in the synthesis strategies and their application in oil-water separation. *Chemical Engineering Journal* **2021**, 405, 127004 (1–30). doi: 10.1016/j.cej.2020.127004.

[8] G. Mendes, M. Faria, A. Carvalho, M. C. Gonçalves, M. N. de Pinho. Structure of water in hybrid cellulose acetate-silica ultrafiltration membranes and permeation properties. *Carbohydrate Polymers* **2018**, 189, 342–351. doi: 10.1016/j.carbpol.2018.02.031.

[9] S. Havriliak, S. Negami. A complex plane representation of dielectric and mechanical relaxation processes in some polymers. *Polymer* **1967**, 8, 161–210. doi: 10.1016/0032-3861(67)90021-3

[10] S. Havriliak, S. Negami. A complex plane analysis of α-dispersions in some polymer systems. *J. Polym. Sci. Part C.* **1966**, 14, 99–117. doi: 10.1002/polc.5070140111

[11] Edited by F. Kremer, A. Schönhals. Broadband dielectric spectroscopy. Berlin: Springer-Verlag; **2003**. ISBN: 9783540434078

[12] D. A. Cerqueira, G. R. Filho, R. M. N. Assunção. A New Value for the Heat of Fusion of a Perfect Crystal of Cellulose Acetate. *Polymer Bulletin* **2006**, 56, 475–484. doi: 10.1007/s00289-006-0511-9

[13] M. Sousa, A. R. Brás, H. I. M. Veiga, F. C. Ferreira, M. N. de Pinho, N. T. Correia, M. Dionísio. Dynamical Characterization of a Cellulose Acetate Polysaccharide. *The Journal of Physical Chemistry B* **2010**, 114(34), 10939–10953. doi:10.1021/jp101665h